Effect of Functionalized SWCNTs on Microstructure of PP-*g*-MA/OMMT/f-SWCNTs Nanocomposite

Yao Gao, Yong Wang, Jing Shi, Shibu Zhu, Yanling Bao, Hongwei Bai, Yanli Li

Key Laboratory of Advanced Technologies of Materials (Ministry of Education), School of Materials Science and Engineering, Southwest Jiaotong University, Chengdu 610031, China

Received 12 February 2008; accepted 4 September 2008
DOI 10.1002/app.29304
Published online 18 February 2009 in Wiley InterScience (www.interscience.wiley.com).

ABSTRACT: The aim of this work was to study the effect of functionalized single-walled carbon nanotubes (f-SWCNTs) on the microstructure of PP-*g*-MA/organic modified montmorillonite (OMMT)/f-SWCNTs ternary nanocomposite. Pristine SWCNTs were chemically modified by maleic anhydride to improve the interaction between PP-*g*-MA and nanotubes. The dispersion states of OMMT in the different nanocomposites were investigated by wide angle X-ray diffraction. The morphologies of the nanocomposites were characterized by scanning electron microscopy. Crystallization behaviors of nanocomposites were studied through differential scanning calorimetry and polarizing optical microscopy. Different than the PP-*g*-MA/OMMT binary nanocomposite, in which the OMMT is mainly in an exfoliated state, the ternary PP-*g*-MA/OMMT/f-SWCNTs nanocomposite exhibits mostly intercalated OMMT. Furthermore, in the ternary nanocomposite, the crystallization of polymer is mainly induced by f-SWCNTs rather than by OMMT.
 J Appl Polym Sci 112: 2413–2424, 2009

Key words: microstructure; PP-*g*-MA/OMMT/f-SWCNTs; crystallization behavior; interaction

INTRODUCTION

The study of nano-reinforced polymeric materials has been intensively carried out in the last decades. The addition of small amounts of nano-sized fillers such as organoclay or carbon nanotubes (CNTs) improves the polymer properties greatly. Good barrier and flame retardant properties, raised heat distortion temperature and excellent mechanical properties have been reported for polymer/organoclay nanocomposites.[1–3] On the other hand, enhanced tensile strength and tensile modulus, toughness, and improved electrical and thermal conductivity have been reported for polymer/CNTs.[4–7]

One of the most studied organoclays is organic modified montmorillonite (OMMT). By selecting the polymer matrix, controlling the blending condition, enhancing compatibility of the composites or introducing shear stress in sample preparation, it is possible to obtain OMMT in, at least, three states in the matrix: intercalated, exfoliated, and coexistence of intercalated and exfoliated states. It is observed that OMMT can greatly affect the crystallization behavior of semicrystalline polymer depending on the state of OMMT in matrix.[8] For the intercalated sample, polymer chains enter the interlayer of OMMT gallery, and in this condition, the crystallization of semicrystalline polymer is confined: longer induction period, longer half-crystallization time, and larger crystallization activation energy are needed than the exfoliated sample.[9] The interfacial interaction between polymer matrix and OMMT is proved to be fundamental to the final state of OMMT in polymer matrix,[10,11] and also to the crystallization behavior of polymer in the nanocomposites.[12,13] A significant work about the interaction of polyolefin nanocomposites based on clay has been done by Misra and coworkers recently.[14,15] They found that the interaction in PE/clay nanocomposites was very weak compared with the interaction in PP/clay nanocomposites, which results in different crystallization behaviors and structures in PE/clay compared with those in PP/clay nanocomposites. For example, clay presents a stronger nucleating effect for PP leading to a significant reduction in spherulites size, whereas in PE/clay system the crystallization temperature and spherulite size remain the same as in pristine PE.

CNTs are widely used as the reinforced filler for polymer nanocomposites with superior mechanical properties. Besides this, CNTs also affect the morphologies of polymer matrix. For example, CNTs act

Correspondence to: Y. Wang (yongwang1976@163.com).
Contract grant sponsor: National Natural Science Foundation of China; contract grant number: 50403019.
Contract grant sponsor: Sichuan Youthful Science and Technology Foundation (P. R. China); contract grant number: 07ZQ026-003.

as a kind of efficient nucleating agent, affecting the crystallization behavior of semicrystalline polymers greatly, and finally induce the decrease of polymer spherulite diameters.[16–24] Under some conditions, CNTs can induce the formation of fibrillar morphology rather than the usual spherulitic one in the nanocomposites.[25–27] However, in some other works, it has been shown that the addition of CNTs doesn't affect the crystallization behavior of polymer matrix.[28] Similar to the nanocomposites with organoclay, the homogeneous dispersion of CNTs is also the most important factor to influence the final properties of polymer/CNTs composites. Surface functionalization is thought to be a very efficient way to improve the dispersion of CNTs in polymer matrix.[29–31]

Although the binary polymer nanocomposites with OMMT or CNTs have been intensively studied, less work has been done to study the ternary polymer nanocomposites with OMMT and CNTs, simultaneously. The work of Peeterbroeck et al.[32] showed that the addition of multiwalled carbon nanotubes (MWCNTs) seemed to limit clay exfoliation. The work of Lu et al.[33] showed a method to prepare novel CNTs-nanoclay composites by direct growth of CNTs on the nanoclay surface. Zhang et al.[34] also prepared a unique 3D nanostructured hybrid filler with the 1D nanotubes growth on 2D clay platelets and the mechanical results showed the significant enhancement effect of the unique 3D nanostructured filler in PA6 nanocomposites.

In this work, the ternary nanocomposite of PP with OMMT and single-walled carbon nanotubes (SWCNTs) was prepared by melt blending. To provide the desired degree of interfacial interaction between nanofillers and polymer matrix, montmorillonite (MMT) was organic modified by dioctadecyl dimethyl ammonium bromide, SWCNTs were grafted by maleic anhydride (f-SWCNTs), and PP modified by maleic anhydride (PP-*g*-MA) was selected as the polymer matrix. The nanocomposites of PP-*g*-MA/OMMT and PP-*g*-MA/f-SWCNTs were also prepared. The microstructures of these nanocomposites were characterized by wide angle X-ray diffraction (WAXD), and the crystallization behaviors were comparatively researched by differential scanning calorimetry (DSC) and polarizing optical microscopy (POM).

EXPERIMENTAL PART

Materials

PP modified by maleic anhydride (PP-*g*-MA) [$M_w = 21.1 \times 10^4$, polydispersity index (d) of 3.2] was obtained from Chengguang Institute of Chemical Engineering, Chengdu, China. MA group was randomly grafted onto a PP backbone, and the MA content in PP was 0.6 wt %. Sodium MMT with a cation exchange capacity of 68.6 nmol/100 g MMT was obtained from Renshou, Sichuan, China. SWCNTs were purchased from Chengdu Institute of Organic Chemistry of the Chinese Academic of Science (Chengdu, China). The average diameter of SWCNTs was 1–2 nm, and the length of single SWCNT was about 50 μm. SWCNTs were washed and purified with concentrated hydrochloride acid, and the purity was above 90% in weight base.

Sample preparation

The organic modification of MMT with dioctadecyl dimethyl ammonium bromide was carried out according to the method in Ref. 35. The chemical modification of SWCNTs with maleic anhydride was carried out as follows: first, SWCNTs were added into concentrated HNO_3 and the mixture was sonicated for 40 min; second, the mixture was stirred at 120°C for 4 h; after that the mixture was filtered through polypropylene membrane with the aperture diameter of 0.2 μm; the solid was washed with distilled water until the pH value of the solution was 7. The filtered nanotubes were dried in an oven under vacuum at 60°C for 24 h to obtain acid-treated SWCNTs (acid-SWCNTs). As a result of the acid modification process, the carboxyl and hydroxyl groups were introduced onto the surface of SWCNTs.[36,37] The acid modified SWCNTs (3 g) were then reacted with maleic anhydride (20 g) in the solution of concentrated HCl and ethyl acetate at 60°C for 5 h (the volume ratio of HCl and ethyl acetate is 1 : 30). Subsequently, SWCNTs were filtered, washed, and dried with the same methods as described earlier. By this method, SWCNTs grafted with maleic anhydride (f-SWCNTs) were finally obtained. The schematic representation of the chemical modification of SWCNTs is shown in Figure 1.

Melt blending of PP-*g*-MA with 2 wt % OMMT (PP-*g*-MA/OMMT_2), PP-*g*-MA with 0.5 wt % SWCNTs-MA (PP-*g*-MA/f-SWCNTs_0.5), and PP-*g*-

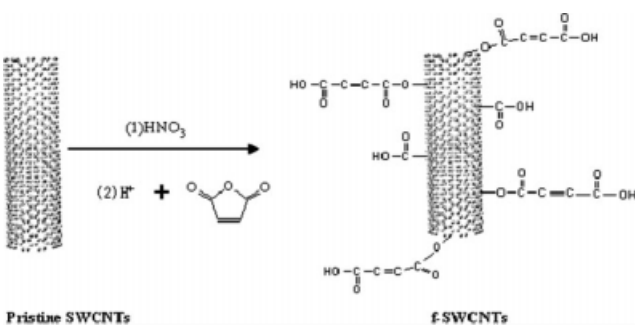

Figure 1 Schematic representation of single-walled carbon nanotubes functionalization process.

MA with 2 wt % OMMT and 0.5 wt % SWCNTs-MA simultaneously (PP-*g*-MA/OMMT_2/f-SWCNTs_0.5) were conducted using a torque rheometer (Shanghai, China) set at a barrel temperature of 190°C and a speed of 70 rpm. Melt-blending time was 8 min.

Characterization

An FTIR equipment model Nicolet 5700 (Madison, USA) was used to characterize the chemical absorption of pristine SWCNTs, chemically modified SWCNTs and PP-*g*-MA nanocomposites. For nanotubes, the sample was directly characterized by FTIR. For nanocomposites, the sample was heated to melt completely and then pressed to obtain a film with a thickness of 20 μm, and the film was characterized by FTIR. FTIR spectrum was recorded from 4000 to 400 cm^{-1} at a resolution of 4 cm^{-1}.

WAXD experiments were conducted using a Panalytical X'pert PRO diffractometer (Almelo, The Netherlands) with Ni-filtered CuKα radiation. The 2θ range was 1–10° with a scanning rate of 1°/min.

Morphologies of OMMT in the nanocomposites were investigated by means of a scanning electron microscope (SEM) Quanta 200 (Eindnoven, The Netherlands), operating at 20 kV. Nanocomposites were fractured in liquid nitrogen.

DSC (Perkin-Elmer Pyris-1, Waltham/Massachusetts, USA) was used to research the isothermal crystallization behaviors of PP-*g*-MA nanocomposites. The instrument was calibrated using indium as standard and the measurement was carried out in nitrogen atmosphere. The sample was quickly heated to 200°C and maintained at this temperature for 10 min to erase the thermal history, then the sample was quickly cooled down to a setting temperature of 128, 130, 132, and 134°C, respectively. The sample was maintained at the setting temperature until the isothermal crystallization was finished completely. A DSC equipment Netzsch STA449C (Selb, Germany) was used to research the nonisothermal crystallization behaviors of PP-*g*-MA nanocomposites. The measurement was conducted as follows: the sample was heated from 30 to 200°C at the heating rate of 10°C /min, maintained at 200°C for 10 min to erase the thermal history. Subsequently, the sample was cooled down to 30°C at the cooling rate of 10°C/min. The measurement was carried out in helium atmosphere.

POM (XPN-203, Shanghai, China) with a hot-stage was used to characterize the isothermal crystallization morphologies of PP-*g*-MA nanocomposites. First, a sample of about 5 mg was placed between two glass slides and was heated to melt completely, and then the sample was pressed to obtain a slice with a thickness of about 20 μm; second, the sample was transferred to the hot-stage set at a temperature of 130°C and maintained at this temperature for 1.5 h. The crystallization morphologies of the samples was recorded with images via a digital camera.

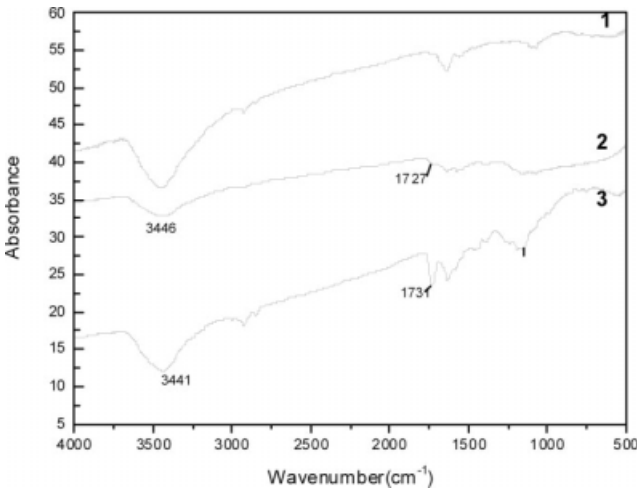

Figure 2 The FTIR spectrums of nanotubes: (1) Pristine SWCNTs, (2) acid-SWCNTs, and (3) f-SWCNTs.

RESULTS AND DISCUSSION

Chemical modification of SWCNTs

Before we research the microstructures of PP-*g*-MA/OMMT/f-SWCNTs nanocomposite, the characterization of chemical modified SWCNTs was carried out initially. FTIR was used to characterize the functionalized SWCNTs. Figure 2 shows the FTIR results of pristine SWCNTs (1), acid-SWCNTs (2), and f-SWCNTs (3). The aim of this work is to introduce maleic anhydride onto the outer surface of SWCNTs, so the absorption band of carbonyl is the main characteristic to evaluate the modification efficiency of SWCNTs. Compared with the FTIR spectrum of pristine SWCNTs, in which there is no absorption band of carbonyl group, the FTIR spectrums of acid-SWCNTs and f-SWCNTs show an apparent absorption band of carbonyl, and the absorption peak position is at 1727 and 1731 cm^{-1}, respectively. Furthermore, one can notice that the absorption peak intensity of carbonyl group of f-SWCNTs is more apparent than that of acid-SWCNTs, which means the increase number of carbonyl groups on f-SWCNTs surface compared with acid-SWCNTs. FTIR spectrum clearly proves that SWCNTs used in this work are successfully functionalized by maleic anhydride.

Microstructures of nanocomposites

The microstructures of nanocomposites were mainly investigated through analyzing the intercalated or exfoliated state of OMMT in the nanocomposites. The WAXD profiles of PP-*g*-MA with different

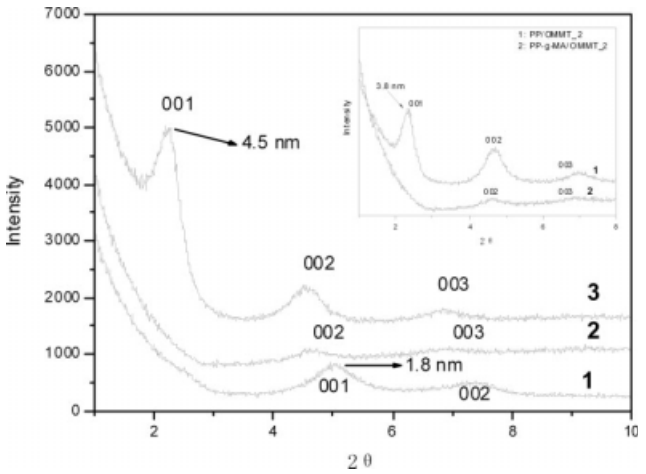

Figure 3 WAXD profiles of (1) OMMT, (2) PP-*g*-MA/OMMT_2, and (3) PP-*g*-MA/OMMT_2/f-SWCNTs_0.5. The inserted graph shows a comparison of WAXD profiles of PP/OMMT_2 and PP-*g*-MA/OMMT_2.

nanofillers are shown in Figure 3. For OMMT (1), the first peak and the second peak correspond to the (001) and (002) reflection of clay (the interlayer gallery height), respectively, and the layer distance of OMMT is 1.8 nm ($2\theta = 5.04$). For PP-*g*-MA/OMMT_2 (2), the (001) reflection disappears, and a very weak (002) and (003) reflections can be observed, which means that the OMMT platelets are mainly exfoliated in the nanocomposite because PP-*g*-MA chains enter into the interlayer of gallery and enlarge the layer distance. The intercalation of PP-*g*-MA into OMMT is easy, so that PP-*g*-MA as a compatibilizer is widely used to improve the compatibility between PP and OMMT.[38,39] To further prove this, the nanocomposite of PP with same content of OMMT was prepared through the same processing method of PP-*g*-MA/OMMT_2 nanocomposite. The inserted graph in Figure 3 shows the comparison of WAXD profiles of PP/OMMT_2 and PP-*g*-MA/OMMT_2 nanocomposites. According to the WAXD profiles, one can clearly know that OMMT is mainly intercalated by PP chains in PP/OMMT_2 nanocomposite and exfoliated in PP-*g*-MA/OMMT_2 nanocomposite.

However, for PP-*g*-MA/OMMT_2/f-SWCNTs_0.5 (3), the characteristic reflection peaks of (001), (002), and (003) of OMMT are very apparent and the layer distance of OMMT is 4.5 nm ($2\theta = 2.28$), which means that the OMMT is mostly intercalated. According to the above results, one can ask whether the presence of a few amounts of f-SWCNTs prevents the exfoliation of OMMT in PP-*g*-MA matrix or not. To confirm this, additional work has been done in this study.

In this work, the preparation of PP-*g*-MA/OMMT_2/f-SWCNTs_0.5 was carried out through blending PP-*g*-MA, OMMT, and f-SWCNTs, simultaneously. It is known to all that the blending sequence of ternary nanocomposites has an important effect on the final microstructure of these systems.[40] Thus, a crucial work that had been done was adjusting the blending sequence of the ternary nanocomposite. The new blending sequence was set as follows: first, PP-*g*-MA was melt blended with 2 wt % OMMT to achieve a high degree of exfoliation of OMMT, then 0.5 wt % f-SWCNTs was introduced into the melt of PP-*g*-MA/OMMT nanocomposite. The melt was further blended to make sure that f-SWCNTs were homogeneously dispersed in the ternary nanocomposite. The samples for WAXD were obtained from the torque rheometer at different blending time after f-SWCNTs were introduced into the melt of PP-*g*-MA/OMMT_2. The corresponding WAXD profiles of such samples are shown in Figure 4. To make a comparison, the WAXD profile of PP-*g*-MA/OMMT_2 (1) after being melt blended for 8 min is also shown in Figure 4. Two minutes after f-SWCNTs being introduced into the blends of PP-*g*-MA/OMMT nanocomposite, the WAXD shows an apparent (001) reflection of OMMT [as shown in Fig. 4(2)], which means that some OMMT are changed from the exfoliated state to the intercalated state. Ten minutes later, the sample shows a very strong (001) reflection of OMMT, [seen in Fig. 4(3)], corresponding to the layer distance of 3.9 nm. Although the layer distance of OMMT has no gradually decrease with the increasing blending time of f-SWCNTs and PP-*g*-MA/OMMT, the reflection intensity increases gradually. This means that, with the increasing blending time, more exfoliated OMMT transforms to intercalated OMMT.

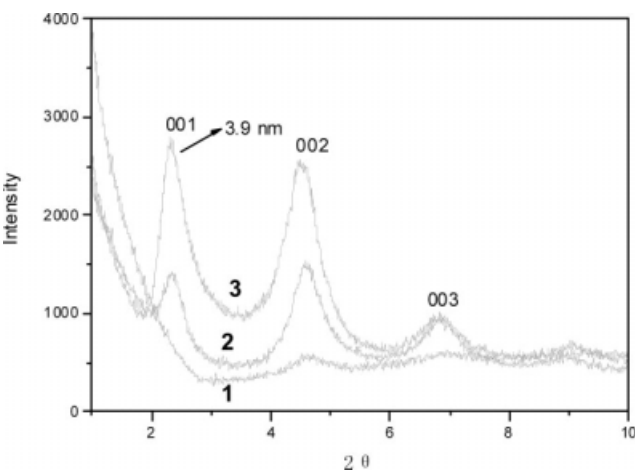

Figure 4 Evolution of WAXD profiles of PP-*g*-MA/OMMT_2/f-SWCNTs_0.5: (1) 8 min after that the PP-*g*-MA and 2 wt % OMMT were first melt blended, (2) 2 min after that the 0.5 wt % f-SWCNTs were introduced into the melt of PP-*g*-MA/OMMT_2, and (3) 10 min after that the 0.5 wt % f-SWCNTs were introduced into the melt of PP-*g*-MA/OMMT_2.

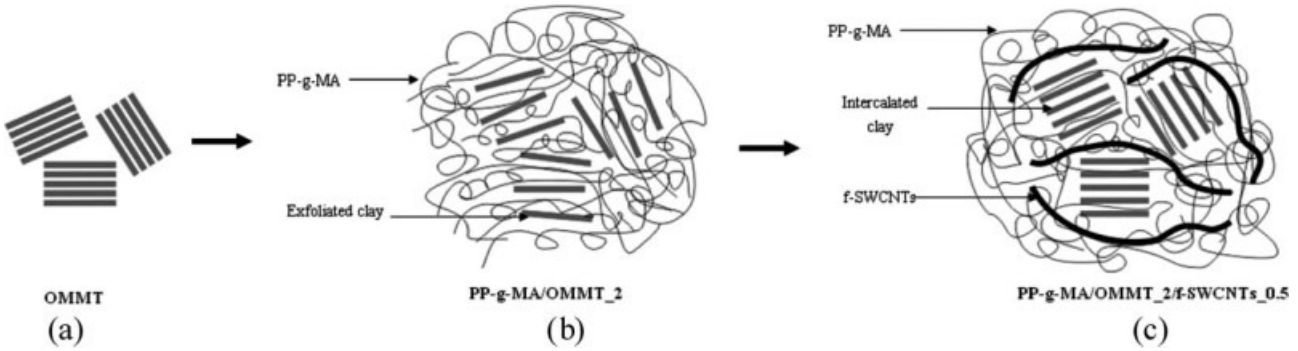

Figure 5 The schematic representations of microstructures in (a) OMMT, (b) PP-*g*-MA/OMMT_2, and (c) PP-*g*-MA/OMMT_2/f-SWCNTs_0.5.

Obviously, the addition of a few amounts of f-SWCNTs really influences the final dispersion state of OMMT in the nanocomposite. For the nanocomposite that are obtained through blending the ternary components, simultaneously, f-SWCNTs prevent more PP-*g*-MA chains to enter into the interlayer of OMMT. For the mainly exfoliated PP-*g*-MA/OMMT nanocomposite, the addition of f-SWCNTs induces those intercalated PP-*g*-MA chains move out from the interlayer of OMMT gallery. Above all, the presence of f-SWCNTs induces the transformation of OMMT microstructure from the exfoliated state to the intercalated state.

The schematic representations of the dispersion state of OMMT in nanocomposites are shown in Figure 5. In PP-*g*-MA/OMMT_2 nanocomposite [Fig. 5(b)], OMMT is mainly exfoliated, but the exfoliated layers of OMMT are not randomly distributed in the matrix, they still keep a certain regular distribution. For example, there is no apparent slippage between two exfoliated layers of OMMT. However, OMMT is mostly intercalated in the PP-*g*-MA/OMMT/f-SWCNTs ternary nanocomposite [Fig. 5(c)].

Morphologies of nanocomposites

As shown in Ref. 35, OMMT treated by dioctadecyl dimethyl ammonium bromide has the polar groups of the alkyl ammonium salt. Both PP-*g*-MA and f-SWCNTs have the polar groups of maleic anhydride. Obviously, the miscibility between PP-*g*-MA and f-SWCNTs is better than that between PP-*g*-MA and OMMT because they have the same functional groups. In other words, the dispersion of f-SWCNTs will be better than that of OMMT in PP-*g*-MA matrix.

The morphologies of OMMT in PP-*g*-MA/OMMT_2 and PP-*g*-MA/OMMT_2/f-SWCNTs_0.5 nanocomposites are shown in Figure 6. For PP-*g*-MA/OMMT_2 nanocomposite [Fig. 6(a)], a good dispersion of OMMT is observed, the primary particle size is about 150–400 nm in length and 30–50 nm in width. However, for PP-*g*-MA/OMMT/f-SWCNTs [Fig. 6(b)], the primary particle size of OMMT is about 250–600 nm in length and 50–240 nm in width. Furthermore, because of the few amounts of f-SWCNTs (only 0.5 wt %) in the ternary nanocomposite and the good miscibility between f-SWCNTs

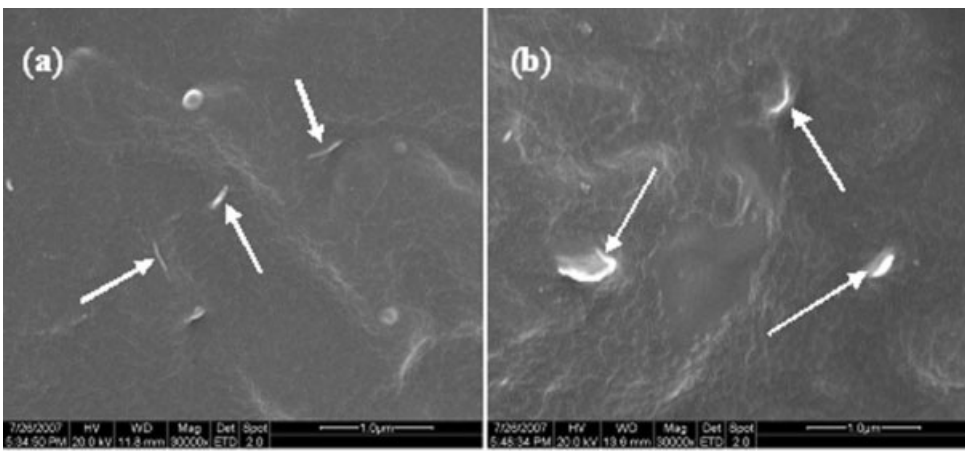

Figure 6 SEM photographs of (a) PP-*g*-MA/OMMT_2 and (b) PP-*g*-MA/OMMT_2/f-SWCNTs_0.5.

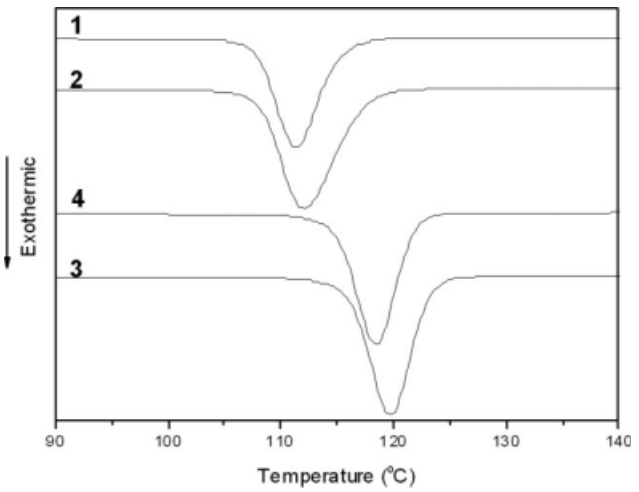

Figure 7 DSC cooling curves of (1) PP-*g*-MA, (2) PP-*g*-MA/OMMT_2, (3) PP-*g*-MA/f-SWCNTs_0.5, and (4) PP-*g*-MA/OMMT_2/f-SWCNTs_0.5.

and matrix, it is very difficult to observe the morphology of f-SWCNTs through our experimental instrument. From Figure 6, one also can see that the addition of f-SWCNTs prevents the good dispersion of OMMT in ternary nanocomposite.

Crystallization behaviors of nanocomposites

To make a clear comparison of crystallization behaviors of PP-*g*-MA with different nanofillers, PP-*g*-MA nanocomposite with 0.5 wt % f-SWCNTs was also prepared and researched in the study. The nonisothermal crystallization behaviors of pure PP-*g*-MA and PP-*g*-MA with different nanofillers are shown in Figure 7 and relative crystallization parameters are shown in Table I. Here T_{onset} and T_c are defined as the initial crystallization temperature and the peak maximum temperature, respectively. ΔH_c is the enthalpy evolved during the crystallization. For PP-*g*-MA/OMMT_2 nanocomposite (2), T_{onset} and T_c are slightly increased from 115.2 and 111.1°C of pure PP-*g*-MA (1) to 117.5 and 112.1°C, respectively, which means a weak nucleation effect of OMMT for PP-*g*-MA crystallization. However, the T_{onset} and T_c of PP-*g*-MA/f-SWCNTs_0.5 nanocomposite (3) are greatly enhanced up to 123.2 and 119.8°C, respectively, indicating a strong nucleation effect of f-SWCNTs. For PP-*g*-MA/OMMT_2/SWCNTs_0.5 (4), both T_{onset} and T_c of the ternary nanocomposite are still much higher than those of PP-*g*-MA and PP-*g*-MA/OMMT_2 nanocomposite but lower than that of PP-*g*-MA/f-SWCNTs_0.5 nanocomposite, which also means an apparent nucleation effect of nanofillers in the ternary nanocomposite. However, it is believed that the nucleation effect of nanofillers is mainly ascribed to f-SWCNTs rather than OMMT in the ternary nanocomposite according to the difference between T_{onset} and T_c of the nanocomposite. The crystallization enthalpy (ΔH_c) of PP-*g*-MA, and, hence, the crystallinity decreases with the presence of nanofillers. This maybe ascribed to the lower mobility of polymer chains in matrix due to the addition of nanofillers. The similar results have been reported by Yuan et al.[14] In their opinion, the dispersed nanoparticles hindered the formation of large crystalline domains in the restricted and confined space.

Figure 8 shows the DSC curves of isothermal crystallization of pure PP-*g*-MA and PP-*g*-MA with different fillers at different temperatures, and Figure 9 shows the variation of relative crystallinity (%) with the crystallization time. From Figures 8 and 9 one can see that, the OMMT has a nucleation effect for PP-*g*-MA during the isothermal crystallization process, but the nucleation effect is much weaker than that of f-SWCNTs. However, compared with the binary nanocomposite of PP-*g*-MA/f-SWCNTs, the maximum crystallization rate position shifts to longer crystallization time and the crystallization peak becomes wider in ternary nanocomposite. To achieve the same relative crystallinity (%), the ternary nanocomposite needs longer crystallization time than PP-*g*-MA/f-SWCNTs binary nanocomposite.

The isothermal crystallization parameters were calculated according to Avrami equation[41,42] and the corresponding results are shown in Figure 10 and Table II. The experimental half-crystallization time ($t^a_{1/2}$) and predicted half-crystallization time ($t^b_{1/2}$) by Avrami analysis are also shown in Table II. For pure polymer, the remnant catalyst may act as the nucleating agent and induces PP-*g*-MA crystallization. For PP-*g*-MA/OMMT_2 nanocomposite, both the crystallization rate constant k and half-crystallization time $t_{1/2}$ show a nucleation effect of OMMT for PP-*g*-MA crystallization. The result is in good agreement with the previous work.[43] For PP-*g*-MA/f-SWCNTs nanocomposite, an apparent increase of k and decrease of $t_{1/2}$ can be obtained due to the great nucleation effect of f-SWCNTs for PP-*g*-MA crystallization. However, for PP-*g*-MA/OMMT_2/f-SWCNTs_0.5

TABLE I
Nonisothermal Crystallization Parameters of PP-*g*-MA and its Nanocomposites

Sample	T_{onset} (°C)	T_c (°C)	ΔH_c[a] (J/g)
PP-*g*-MA	115.2	111.1	48.2
PP-*g*-MA/OMMT_2	117.5	112.0	45.2
PP-*g*-MA/f-SWCNT_0.5	123.2	119.8	42.0
PP-*g*-MA/OMMT_2/f-SWCNT_0.5	121.8	118.5	40.3

T_{onset}, initial crystallization temperature; T_c, peak maximum temperature; ΔH_c: crystallization enthalpy.
[a] For 100 wt % polymer.

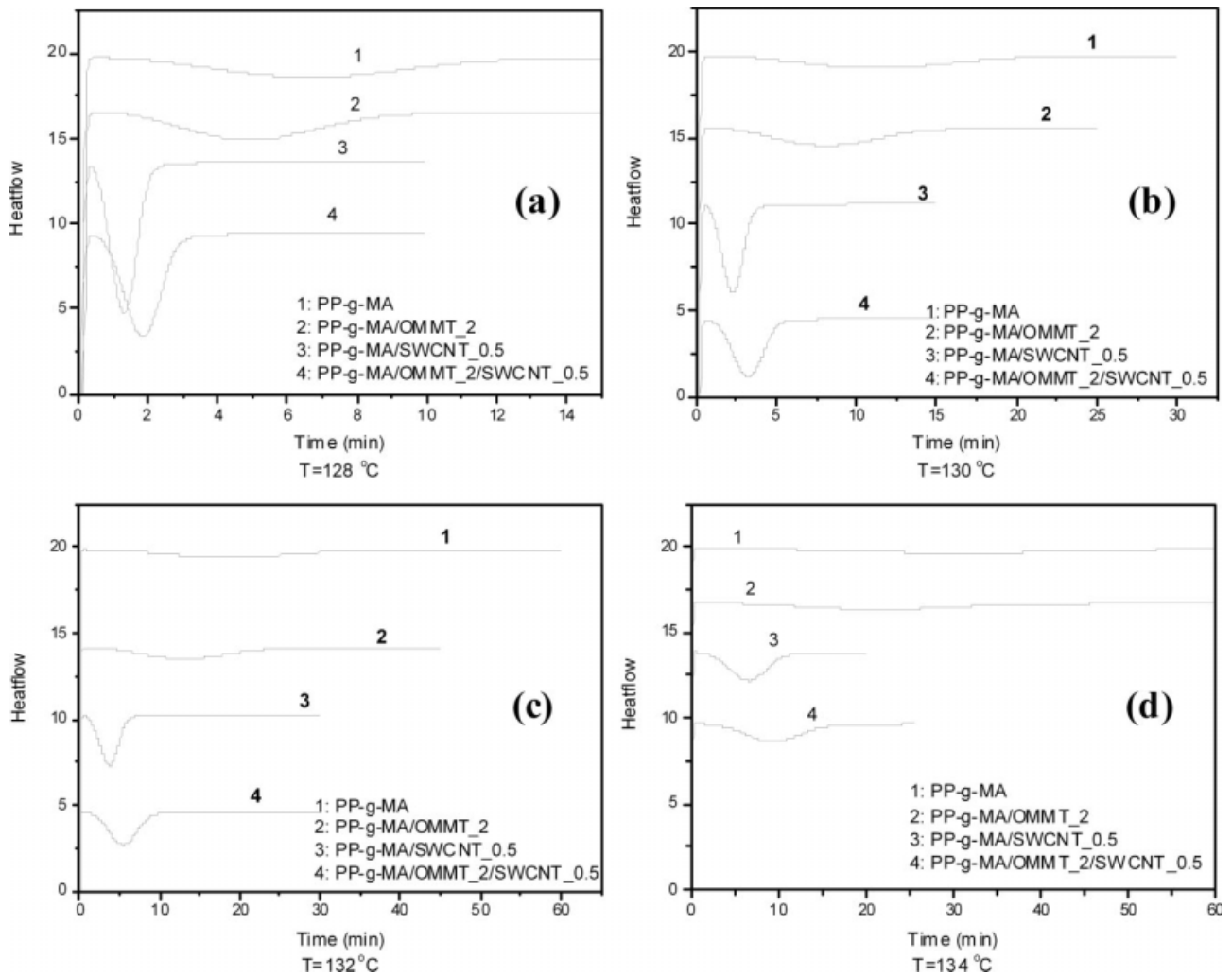

Figure 8 The isothermal crystallization curves of PP-*g*-MA with different fillers obtained at different temperatures: (a) 128°C, (b) 130°C, (c) 132°C, and (d) 134°C.

nanocomposite, compared with the values of k and $t_{1/2}$ of the binary nanocomposites of PP-*g*-MA/OMMT_2 and PP-*g*-MA/f-SWCNTs_0.5, the crystallization parameters of the ternary nanocomposite show that the crystallization rate is higher than that of PP-*g*-MA/OMMT_2 but lower than that of PP-*g*-MA/f-SWCNTs_0.5. The results are in good agreement with the nonisothermal crystallization results. Considering the dispersion state of OMMT in the nanocomposites, one can believe that the addition of f-SWCNTs can greatly increase the crystallization rate of PP-*g*-MA, but the existence of intercalated OMMT layers confines the motion of PP-*g*-MA chain segments.[9] On the other hand, a value close to 3 for the Avrami exponent implies that spherulitic development arises from an athermal heterogeneous nucleation. The addition of nanofillers does not practically affect the Avrami exponent of polymer matrix. The similar results have been reported by other researchers.[24]

Figure 11 shows the plots of the inverse of $t_{1/2}^{a}$ versus isothermal crystallization temperature. It is clearly observed that the crystallization kinetics of PP-*g*-MA with OMMT is similar to that of pure polymer. The presence of f-SWCNTs greatly affect the crystallization kinetics of matrix. However, in the ternary nanocomposites, the presence of OMMT prevents the crystallization of matrix.

Figure 12 shows the crystallization morphologies of PP-*g*-MA with different nanofillers which were obtained through POM. For pure PP-*g*-MA [Fig. 12(a)], big spherulites are observed. The spherulites are not homogeneous and the diameters of spherulites vary from 50 to 200 μm. For PP-*g*-MA/OMMT_2 nanocomposite [Fig. 12(b)], smaller spherulites are observed, and the average diameter of spherulites is about 100 μm. Much smaller and homogeneous spherulites are observed in PP-*g*-MA/f-SWCNTs_0.5 nanocomposite [Fig. 12(c)], and the average diameter of spherulites is only about 25 μm.

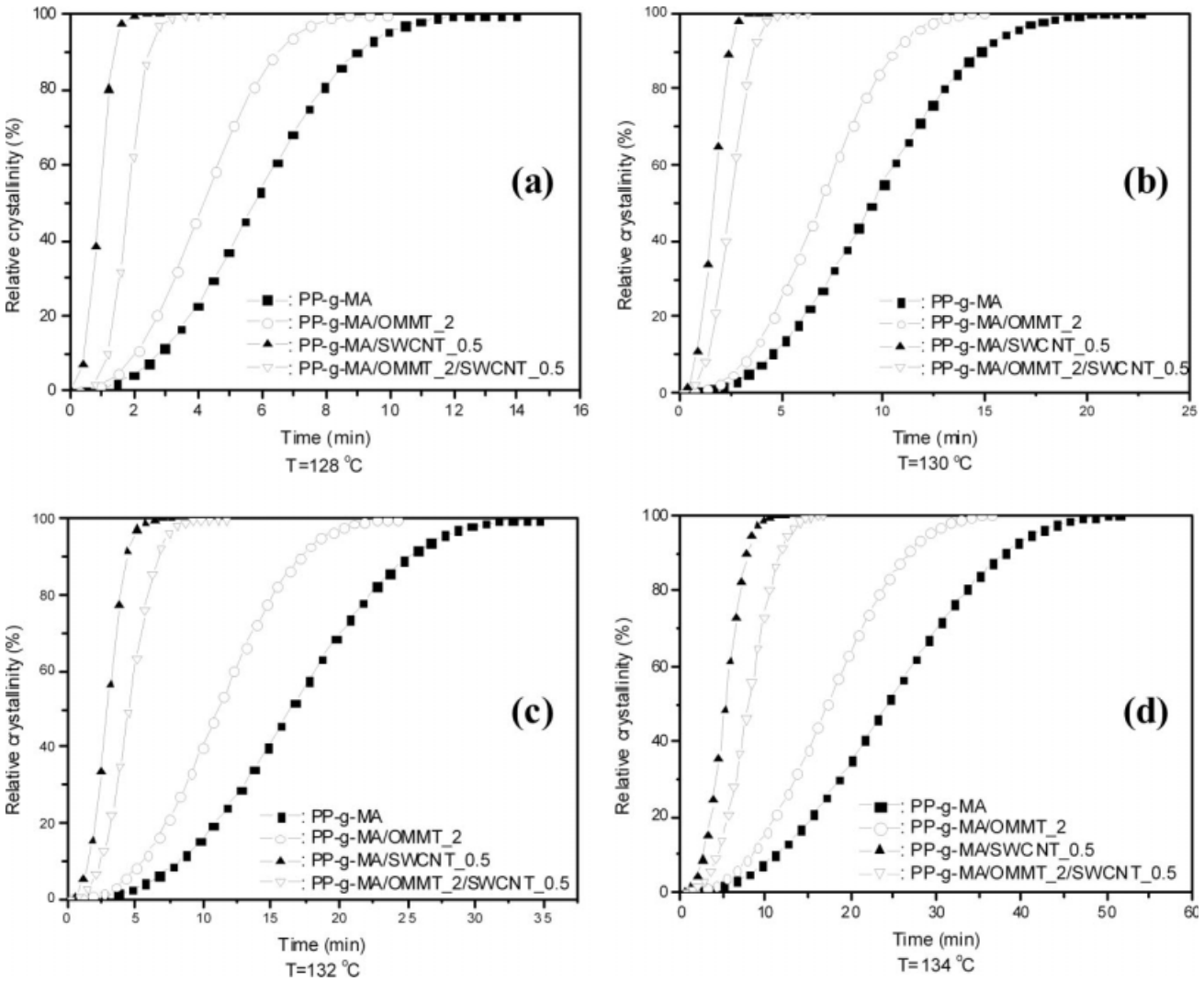

Figure 9 Evolution of the relative crystallinity (%) in PP-*g*-MA with different fillers as a function of crystallization time and temperature: (a) 128°C, (b) 130°C, (c) 132°C, and (d) 134°C.

This indicates the apparent nucleation effect of f-SWCNTs for PP-*g*-MA crystallization. However, for the ternary nanocomposite [Fig. 12(d)], the spherulites are slightly larger than those of PP-*g*-MA/f-SWCNTs_0.5 but still much smaller than those of PP-*g*-MA/OMMT_2 nanocomposite. The results obtained through POM are in good agreement with the results obtained through DSC.

Interfacial interactions of nanocomposites

It is known to all that the interfacial interaction plays a critical role in the free energy of cluster formation and the rate of nucleation. The weak interaction lowers the rate of nucleation.[12,13] According to the above results, one can believe that the interfacial interaction between PP-*g*-MA and f-SWCNTs is stronger than that between PP-*g*-MA and OMMT. For PP-*g*-MA/OMMT system, the interfacial interaction is mainly attributed to the hydrogen bonding between the maleic anhydride groups on PP-*g*-MA chains and alkyl ammonium groups in OMMT gallery. For the PP-*g*-MA/f-SWCNTs system, the interfacial interaction is mainly attributed to the good miscibility between the components and to the template effect of f-SWCNTs in the PP-*g*-MA crystallization.

The interaction between the two components can be characterized through the shifts in the corresponding bands of the FTIR spectrum.[44,45] The FTIR spectrums of pure and nanofillers filled PP-*g*-MA were obtained using KBr pelleting method and the results are shown in Figure 13. Similar to the evaluation of chemical modification of SWCNTs, the shift of absorption band of carbonyl is also the main characteristic to prove the interaction between PP-*g*-MA

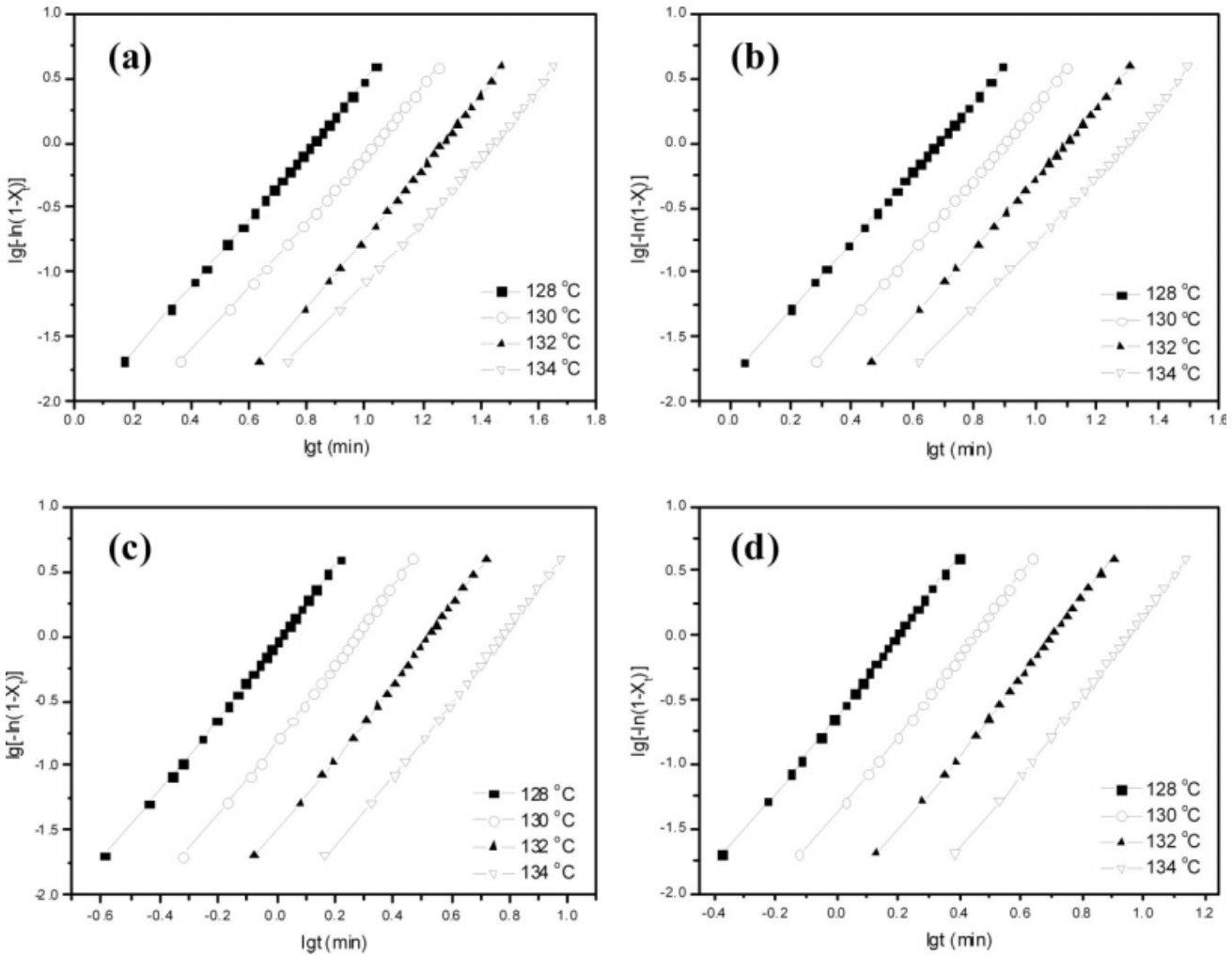

Figure 10 Avrami plots of $1g[-\ln(1 - X_t)]$ versus $1gt$: (a) PP-*g*-MA, (b) PP-*g*-MA/OMMT_2, (c) PP-*g*-MA/f-SWCNTs_0.5, and (d) PP-*g*-MA/OMMT_2/f-SWCNTs_0.5.

TABLE II
Crystallization Parameters of PP-*g*-MA and its Nanocomposites Obtained via Isothermal Crystallization

Sample	T (°C)	n	$1gk$	k ($\times 10^{-3}$) (min^{-1})	$t_{1/2}^{a}$ (min)	$t_{1/2}^{b}$ (min)
PP-*g*-MA	128	2.58	−2.14	7.22	5.80	5.6
	130	2.49	−2.61	2.46	9.48	9.64
	132	2.64	−3.40	0.40	16.52	16.75
	134	2.34	−3.43	0.37	24.27	25.00
PP-*g*-MA/OMMT_2	128	2.69	−1.83	14.80	4.19	4.18
	130	2.74	−2.47	3.42	6.94	6.95
	132	2.64	−2.93	1.16	11.16	11.23
	134	2.47	−3.25	0.57	17.45	17.69
PP-*g*-MA/f-SWCNT_0.5	128	2.75	−0.09	810	0.93	0.95
	130	2.82	−0.82	150	1.66	1.71
	132	2.78	−1.52	30	2.94	3.11
	134	2.75	−2.19	6.45	5.34	6.62
PP-*g*-MA/OMMT_2/f-SWCNT_0.5	128	2.94	−0.63	230	1.84	1.45
	130	2.96	−1.38	40	2.52	2.58
	132	2.93	−2.12	7.66	4.52	4.65
	134	3.03	−2.91	1.23	7.96	8.09

T, isothermal crystallization temperature; n, Avrami exponent; k, crystallization rate constant; $t_{1/2}^{a}$, experimental half-crystallization time; $t_{1/2}^{b}$: predicted half-crystallization time by Avrami analysis.

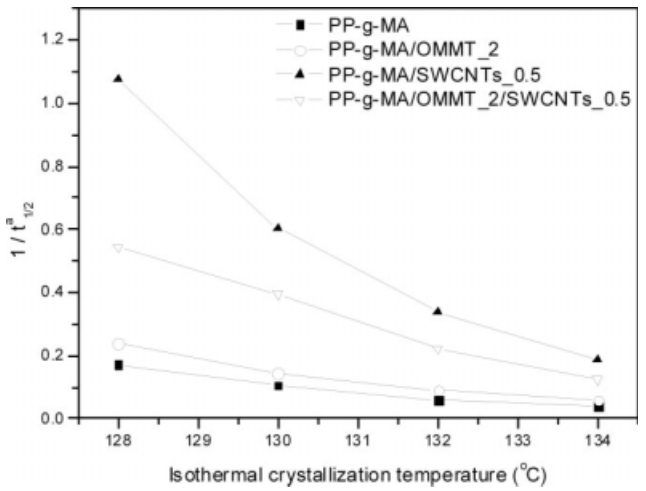

Figure 11 Inverse of the experimental half-crystallization time ($t^a_{1/2}$) versus isothermal crystallization temperature for PP-*g*-MA with different fillers.

and nanofillers. For pure PP-*g*-MA (1), the main absorption band of carbonyl is at 1713 cm^{-1}. For PP-*g*-MA/OMMT_2 nanocomposite (2), the corresponding absorption band of carbonyl shifts to 1717 cm^{-1} with a change in intensities. This indicates the considerable interaction between PP-*g*-MA and OMMT. This effect can also be invoked to explain why OMMT is mainly in an exfoliated state in the PP-*g*-MA/OMMT nanocomposite. For PP-*g*-MA/f-SWCNTs_0.5 (3), the FTIR spectrum shows no change in the corresponding band due to the same functional groups of PP-*g*-MA and f-SWCNTs. However, for the ternary nanocomposite of PP-*g*-MA/OMMT_2/f-SWCNTs_0.5 (4), the FTIR spectrum shows the similar absorption band of carboxyl compared with PP-*g*-MA/OMMT_2 nanocomposite, which also indicates the available interaction between maleic anhydride groups and alkyl ammonium groups.

FTIR doesn't show the interaction between PP-*g*-MA and f-SWCNTs because of the same functional groups of them. Another experiment had been carried out to prove how the interaction between PP-*g*-MA and f-SWCNTs affect the microstructure of the nanocomposite. The pristine SWCNTs were blended with PP-*g*-MA and OMMT, simultaneously, and the

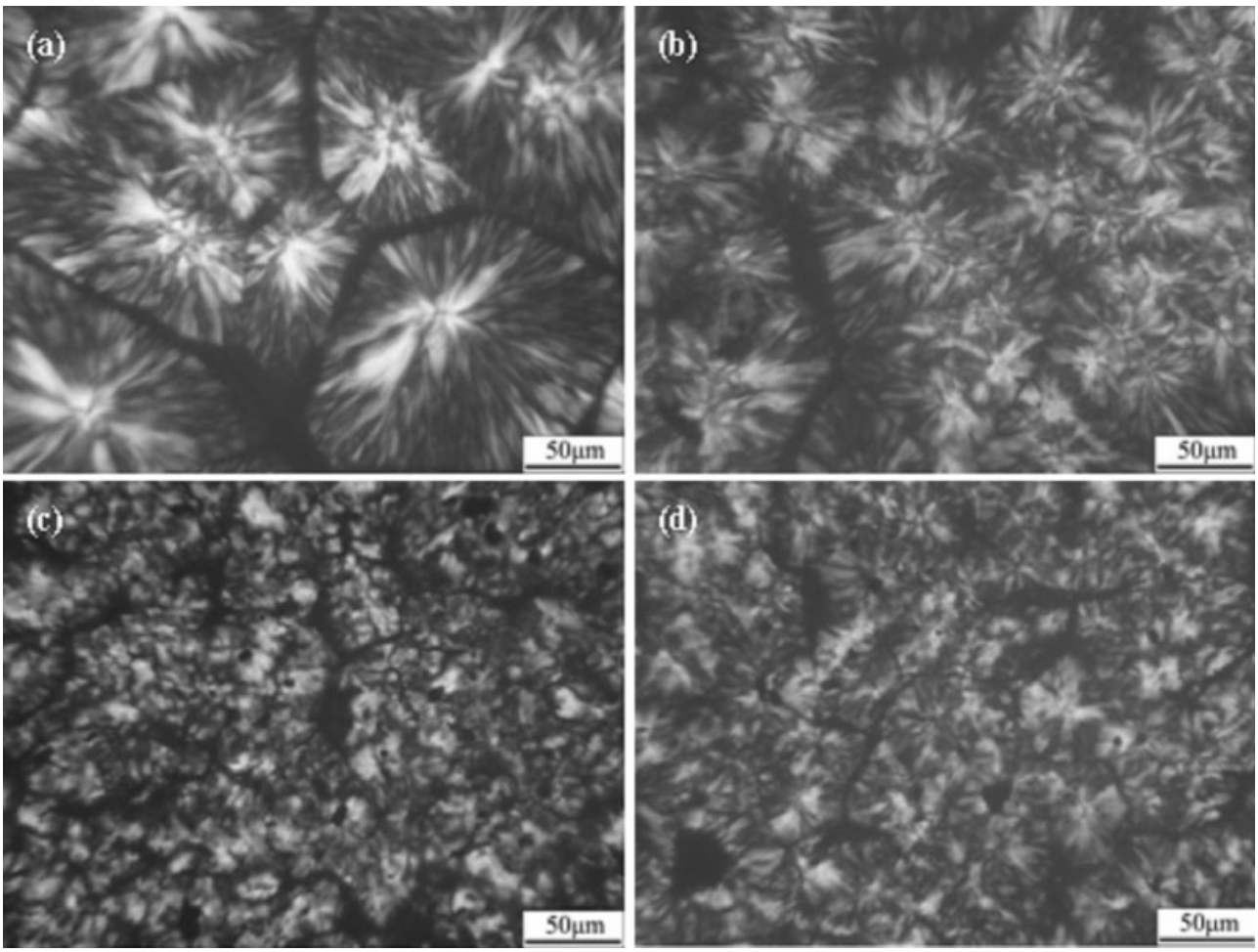

Figure 12 POM photographs of (a) PP-*g*-MA, (b) PP-*g*-MA/OMMT_2, (c) PP-*g*-MA/f-SWCNTs_0.5, and (d) PP-*g*-MA/OMMT_2/f-SWCNTs_0.5. The isothermal crystallization temperature was 130°C.

dispersion state of OMMT in this nanocomposite was also characterized by WAXD. Figure 14 shows a comparison of WAXD profiles among PP-MA/OMMT_2 (1), PP-*g*-MA/OMMT_2/pristine SWCNTs (2), and PP-*g*-MA/OMMT_2/f-SWCNTs (3). From this figure one can notice that the addition of pristine SWCNTs has no apparent influence on the dispersion state of OMMT. OMMT still keeps the exfoliated state in the ternary nanocomposite. So, it can be concluded that the transformation of OMMT dispersion state from the exfoliate state to the intercalated state is mainly due to the addition of functionalized SWCNTs.

In fact, since the samples were characterized through the off-line way rather than the in-line way, the obtained results from WAXD can not really reflect the dispersion state of OMMT in the melt. It can be hypothesized that the role of f-SWCNTs in ternary nanocomposite includes at least two possibilities. One possibility is the addition of f-SWCNTs prevents more PP-*g*-MA chains to enter into the interlayer of OMMT gallery, in this condition, OMMT is mostly melt intercalated by few PP-*g*-MA chain segments. The other possibility is that during the melt blending, the exfoliation of OMMT is available due to the shear stress and the good interaction between PP-*g*-MA and OMMT, and the OMMT is mainly in the exfoliated state in the melt. However, during the cooling process, the great template effect and strong nucleation effect of f-SWCNTs for PP-*g*-MA crystallization induces the PP-*g*-MA chain segments which inserted into the interlayer of OMMT move out from the gallery, and in this condition only few PP-*g*-MA chain segments maintain in the interlayer, thus OMMT is mostly intercalated in the ternary nanocomposite. For the ternary nanocomposite with pristine SWCNTs, the WAXD results show

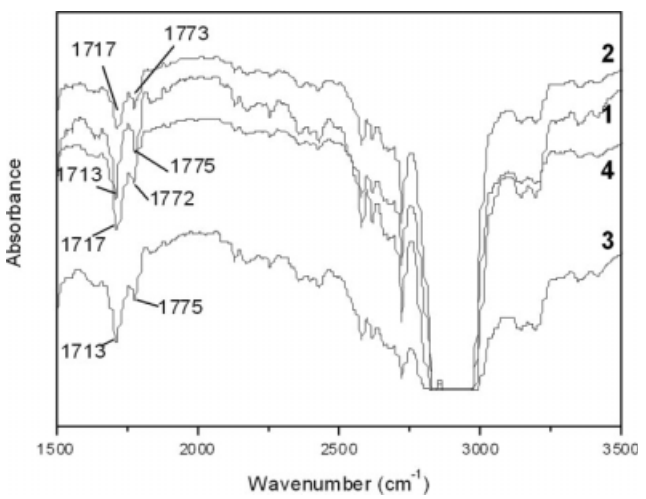

Figure 13 FTIR spectrums of (1) PP-*g*-MA, (2) PP-*g*-MA/OMMT_2, (3) PP-*g*-MA/f-SWCNTs_0.5, and (4) PP-*g*-MA/OMMT_2/f-SWCNTs_0.5.

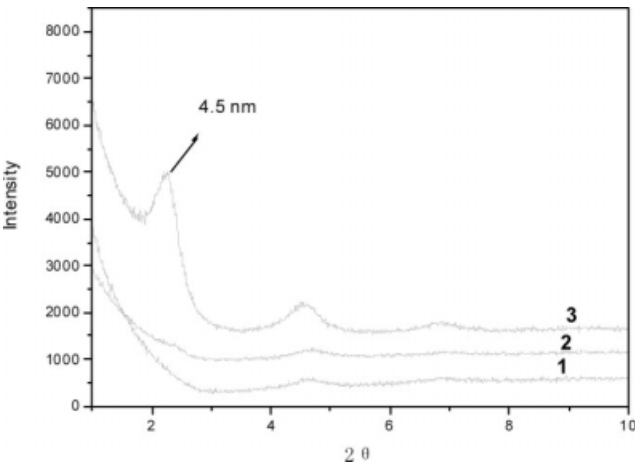

Figure 14 WAXD profiles of (1) PP-*g*-MA/OMMT_2, (2) PP-*g*-MA/OMMT_2/pristine-SWCNTs_0.5, and (3) PP-*g*-MA/OMMT_2/f-SWCNTs_0.5.

that OMMT are mainly exfoliated (seen in Fig. 14). However, previous work performed by other researchers has shown that pristine SWCNTs have an effective nucleation effect for PP crystallization.[46–48] This seems in contradiction with our results. But one should notice that the dispersion of pristine SWCNTs is very poor in the nanocomposites, most of SWCNTs are aggregated and can not prevent the enter of PP-*g*-MA chains into the interlayer of OMMT gallery due to the hydrogen bonding effect between PP-*g*-MA and OMMT and the poor miscibility between PP-*g*-MA and pristine SWCNTs. During the crystallization process, even if pristine SWCNTs have an effective nucleation effect for PP-*g*-MA crystallization and induce the chains without maleic anhydride groups to crystallize, those chains with maleic anhydride groups are still maintaining in the interlayer of OMMT gallery. Thus, part of the OMMT is still in the exfoliated state in such nanocomposite. To investigate the actual role of f-SWCNTs in the ternary nanocomposite, additional work should be done in the future, for example, using in-line WAXD to investigate the dispersion state of OMMT in the melt and using high resolution TEM to characterize the microstructure of OMMT and f-SWCNTs in the solid state.

CONCLUSION

In summary, the microstructures in PP-*g*-MA binary and ternary nanocomposites have been comparatively studied. In PP-*g*-MA/OMMT_2 nanocomposite, OMMT is mainly in the exfoliated state and the exfoliated OMMT platelets have nucleation effect for PP-*g*-MA crystallization, especially during the isothermal crystallization process. The addition of a few amounts of f-SWCNTs prevents the exfoliation of OMMT, and OMMT is mostly in the intercalated

state in the ternary nanocomposite. f-SWCNTs have more apparent nucleation effect in inducing PP-*g*-MA crystallization, but the existence of the intercalated OMMT confines the motion of PP-*g*-MA chain segments. The results show that interfacial interaction between matrix and the nanofiller is very important in determining the microstructure of the ternary nanocomposite.

The authors thank Dr. Qin Zhang, Sichuan University, China, for useful discussion.

References

1. Konstantinos, G. G.; József, K. K. Euro Polym J 2007, 43, 1097.
2. Cho, J. W.; Paul, D. R. Polymer 2000, 42, 1083.
3. Lee, J. H.; Jung, D.; Hong, C. E.; Rhee, K. Y.; Adami, S. G. Comp Sci Tech 2005, 65, 1996.
4. Liu, L.; Barber, A. H.; Nuriel, S.; Wagner, H. D. Adv Funct Mater 2005, 15, 975.
5. Kim, J. K.; Park, H. S.; Kim, S. H. J Appl Polym Sci 2007, 103, 1450.
6. Hu, G.; Zhao, C.; Zhang, S. M.; Yang, M. S.; Wang, Z. G. Polymer 2006, 47, 480.
7. Jeon, K.; Lumata, L.; Tolumoto, T.; Steven, E.; Brools, J.; Alamo, R. G. Polymer 2007, 48, 4751.
8. Homminga, D.; Goderis, B.; Dolbnya, I.; Groeninckx, G. Polymer 2006, 47, 1620.
9. Xu, J. T.; Zhao, Y. Q.; Wang, Q.; Fan, Z. Q. Polymer 2005, 46, 11978.
10. Osman, M. A.; Rupp, J. E. P. Marcomol Rapid Commun 2005, 26, 880.
11. Miltner, H. E.; Peeterbroeck, S.; Viville, P.; Dubois, P.; Mele, B. V. J Polym Sci Part B: Polym Phys 2007, 45, 1291.
12. Tanniru, M.; Yuan, Q.; Misra, R. D. K. Polymer 2006, 47, 2133.
13. Yuan, Q.; Misra, R. D. K. Polymer 2006, 47, 4421.
14. Yuan, Q.; Awate, S.; Misra, R. D. K. J Appl Polym Sci 2006, 102, 3809.
15. Deshmane, C.; Yuan, Q.; Perkins, R. S.; Misra, R. D. K. Mater Sci Eng A 2007, 458, 150.
16. Phang, I. Y.; Ma, J. H.; Liu, T. X.; Zhang, W. D. Polym Int 2006, 55, 71.
17. Kim, J. Y.; Park, H. S.; Kim, S. H. Polymer 2006, 47, 1379.
18. Trujillo, M.; Arnal, M. L.; Mueller, A. J.; Laredo, E.; Bredeau, St.; Bonduel, D.; Dubois, Ph. Macromolceules 2007, 40, 6268.
19. Chen, Q.; Bin, Y.; Matsuo, M. Macromolecules 2006, 39, 6528.
20. Probst, O.; Moore, E. M.; Resasco, D. E.; Grady, B. P. Polymer 2004, 45, 4437.
21. Grady, B. P.; Pompeo, F.; Shambaugh, R. L.; Resasco, D. E. J Phys Chem B 2002, 106, 5852.
22. Mitchell, C. A.; Krishnamoorti, R. Polymer 2005, 46, 8796.
23. Bin, Y.; Kitanaka, M.; Zhu, D.; Matsuo, M. Macromolecules 2003, 36, 6213.
24. Bhattacharyya, A. R.; Sreekumar, T. V.; Liu, T.; Kumar, S.; Ericson, L. M.; Hauge, R. H.; Smalley, R. E. Polymer 2003, 44, 2373.
25. Haggenmueller, R.; Fischer, J. E.; Winey, K. I. Macromolecules 2006, 39, 2964.
26. Minus, M. L.; Chae, H. G.; Kumar, S. Polymer 2006, 47, 3705.
27. Assouline, E.; Lustiger, A.; Barber, A. H.; Cooper, C. A.; Klein, E.; Wachtel, E.; Wagner, H. D. J Polym Sci Part B: Polym Phys 2003, 41, 520.
28. Goh, H. W.; Goh, S. H.; Xu, G. Q.; Pramoda, K. P.; Zhang, W. D. Chem Phys Lett 2003, 379, 236.
29. Saito, T.; Matsushige, K.; Tanaka, K. Phys B 2002, 323, 280.
30. Shieh, Y. T.; Liu, G. L.; Hwang, K. C.; Chen, C. C. Polymer 2005, 46, 10945.
31. Kim, J. A.; Seong, D. G.; Kang, T. J.; Youn, J. R. Carbon 2006, 44, 1898.
32. Peeterbroeck, S.; Alexandre, M.; Nagy, J. B.; Moreau, N.; Destree, A. Macromol Symp 2005, 221, 115.
33. Lu, M.; Lau, K. T.; Qi, J. Q.; Zhao, D. D.; Wang, Z.; Li, H. L. J Mater Sci 2005, 40, 3545.
34. Zhang, W. D.; Phang, I. Y.; Liu, T. X. Adv Mater 2008, 18, 73.
35. Wang, Y.; Zhang, Q.; Fu, Q. Macromol Rapid Commun 2003, 24, 231.
36. Andrews, R.; Jacques, D.; Rao, A. M.; Derbishire, F.; Qian, D.; Fan, X.; Dicky, E. C.; Chen, J. Chem Phys Lett 1991, 303, 467.
37. Kyotani, T.; Nakazaki, S.; Xu, W. H.; Tomita, A. Carbon 2001, 39, 783.
38. Zhang, Q.; Wang, Y.; Fu, Q. J Polym Sci Part B: Polym Phys 2003, 41, 1.
39. Xu, W. B.; Liang, G. D.; Zhai, H. B.; Tang, S. P.; Hang, G. P.; Pan, W. P. Euro Polym J 2003, 39, 1467.
40. Dasari, A.; Yu, Z. Z.; Mai, Y. W. Polymer 2005, 46, 5986.
41. Avrami, M. J. Chem Phys 1940, 8, 212.
42. Jeziorny, A. Polymer 1978, 19, 1142.
43. Li, J.; Zhou, C.; Gamg, W. Polym Test 2003, 22, 217.
44. Wan, T.; Clifford, M. J.; Gao, F.; Bailey, A. S.; Gregory, D. H.; Somsunan, R. Polymer 2005, 46, 6429.
45. Bhajantri, R. F.; Ravindrachary, V.; Harisha, A.; Crasta, V.; Nayak, S. P.; Poojary, B. Polymer 2006, 47, 3591.
46. Valentini, L.; Biagiotti, J.; Kenny, J. M.; López Manchado, M. A. J Appl Polym Sci 2003, 89, 2657.
47. Leelapornpisit, W.; That, M. T. T.; Sarazin, F. P.; Cole, K. C.; Denault, J.; Simard, B. J Polym Sci Part B: Polym Phys 2005, 43, 2445.
48. Seo, M. K.; Lee, J. R.; Park, S. J. Mater Sci Eng A 2005, 404, 79.